A model of the W/Cu interface in the ITER cooling monoblocks from Density Functional Theory

Yosvany Silva Solís, Julien Denis, Etienne A Hodille, Y Ferro

A model of the W/Cu interface in the ITER cooling monoblocks from Density Functional Theory.

Y. Silva-Solís[a], J. Denis[a], E. A. Hodille[b] and Y. Ferro[a,*]

[a]Aix-Marseille University, CNRS, PIIM, F-13013 Marseille, France.

[b]CEA, IRFM, F-13108 Saint-Paul-lez-Durance, France.

*Corresponding author: yves.ferro@univ-amu.fr

Abstract

ITER divertor is built with tungsten monoblocks that contain a tunsgten-copper interface. There, hydrogen isotopes could possibly accumulate leading to safety and mechanical issues. As a consequence, the tunsgten-copper interface has to be modeled and characterized, which is here performed at the atomic-scale by means of density functional theory calculations. In order to build the model, we selected the tungsten and copper orientations that minimizes the mismatch between both networks; this results in the W(001)/Cu^{bcc}(001) and W(001)/Cu^{fcc}(001)R45° interfaces. After relaxation, both systems converge to the same W^{bcc}(001)/Cu^{hcp}(11$\bar{2}$0) structure, which is consistent with previous experimental observations. Such reconstruction of the copper network has the effect of changing the charge density in the copper part of the interface, with possible effects on hydrogen interaction.

Keywords: interface, DFT, reconstruction, charge density.

1 Introduction

In fusion devices such as ITER and DEMO, transport and retention of hydrogen isotopes (HIs) in plasma-facing components (PFCs) can lead to the formation of defects, fuel loss and degradation of the tokamak performance [1, 2]. The PFCs of the divertor in ITER and WEST are built using tungsten (W) monoblocks [3]. The pipes inside the PFCs are made of a copper-chromium-zirconium (CuCrZr), whereas a copper (Cu) inter-layer is used to minimize the mechanical stress between W and CuCrZr [4]. This work specifically focuses on the W/Cu interface where HIs could possibly accumulate and stabilize and/or induce new types of defects. It is led at the atomic scale and is based on density functional theory (DFT) calculations. A model of the W/Cu interface is built with the main goal to determine the structural changes induced by the interface on the W and Cu structures. As an infinite number of W/Cu interfaces can be built considering different crystallographic plane orientations, we restricted this investigation by considering the two orientations for which experimental observations exist [5, 6] and which have the lowest mismatch parameters between W and Cu networks [7, 8]. This resulted in the W(001)/Cu^{bcc}(001) and W(001)/Cu^{fcc}(001)R45° models. This work constitutes a first step before evaluating the solution, segregation and diffusion properties of HIs at the W/Cu interface.

2 Methodology

2.1 Details of the electronic structure calculations

Our electronic structure calculations were done with the Quantum Espresso open-source package [9]. We employed ultrasoft pseudopotentials (USPP) with 14 valence and semi-core electrons for W atoms ($5s^2 5p^6 5d^4 6s^2$) and 11 valence electrons for Cu atoms ($4s^2 3d^9$), both of them were generated with the

PBE-GGA [10] exchange-correlation functional. We used a cutoff energy value of 45 Ry and 360 Ry for the plane-waves and electronic density expansions, respectively. The working-cell contains 64 atoms (32 Cu and 32 W atoms); it was built with a $2 \times 2 \times 8$ repetition of the Cu and W unit-cells, which is detailed later on in this paper. Since a pseudo-2D model is built in the (X, Y) plane, the Brillouin zone was sampled with $10 \times 10 \times 1$ mesh of k-points. The calculated cell parameters for the Cu^{fcc} and Cu^{bcc} bulks structures are 3.620 Å and 2.871 Å, respectively. The cell parameter for W^{bcc} bulks structures was determined to 3.187 Å in a previous paper [11].

2.2 Building a W/Cu interface model

The difference between the cell parameters of W and Cu makes it difficult to build a model of the interface. From one hand the Cu part can be thought as being grown in epitaxy with the $W^{bcc}(001)$ surface leading to the formation of pseudomorphic Cu layers of bcc structure [6, 8, 12]. It can also be thought as having the same fcc structure as Cu in its most stable symmetry. Previous authors built similar W/Cu interface models considering a substrate metal, most often W, with the other metal deposited on top of it [13–15]. Each metallic part consists in several atomic 2D layers. In these previous works, the in-plane cell-parameters were fixed by the substrate, while the full W/Cu bilayer was separated from its repeated image by a vacuum of 10-20 Å. Such a model has one interface, two metallic surfaces, and is akin to dipole moment induced by the two different metals.

In the present work, the full geometry and volume of the working-cell are relaxed: starting from a mean-value of the Cu and W cell-parameters, we led a full geometry optimization of the atomic positions and of the cell-parameters to find the geometry of lowest energy. In addition, we consider no vacuum, making the working-cell separated from its repeated image by another W/Cu interface. As a consequence the pseudo-2D working-cell contains two W/Cu interfaces, no metallic surface and no vacuum.

We investigated two systems: $W(001)/Cu^{bcc}(001)$ for Cu grown in epitaxy over the W(100) surface, and $W(001)/Cu^{fcc}(001)R45°$ that keeps the same symmetry as Cu in its bulk geometry. In the latter case, the fcc structure was rotated by 45° (Figure 1) such as the (002) surface of Cu continues the W^{bcc} network (or in other words, the [100] direction of W^{bcc} and the $[1\bar{1}0]$ direction of Cu^{fcc} are collinear). The thickness of both $W(001)/Cu^{bcc}(001)$ and $W(001)/Cu^{fcc}(001)R45°$ super-cells is given by n_z, which represents the total number of cells in the Z direction: $n_z = N_{Cu} + N_W$, with N_{Cu} and N_W being the number of cells in the Cu and W networks, respectively. We fixed $N_{Cu} = N_W = N$ and, therefore, $n_z = 2N$. In addition; it is known that the W(100) surface reconstructs. Such a surface reconstruction requires a 2×2 unit-cell in the (X, Y) plane to be modeled [16, 17]. Because this surface reconstruction certainly plays a role in the structure of the W/Cu interface, we used a $(2 \times 2 \times n_z)$ model.

To find the optimal size of the system, the value of N was changed from 1 to 7. In the case of $W(001)/Cu^{bcc}(001)$, the initial cell parameters used to build the super-cell were: $a_{W/Cu^{bcc}} = b_{W/Cu^{bcc}} =$ 3.029 Å, $c_{W/Cu^{bcc}} = 2.871$ Å in the Cu network and $c_{W/Cu^{bcc}} = 3.187$ Å in the W network. Where a, b and c represent the unit-cell parameters in X, Y and Z directions respectively. Thus, the $W(001)/Cu^{bcc}(001)$ resulted in a super-cell of size (6.06 Å × 6.06 Å × 6.06N Å). To create the $W(001)/Cu^{fcc}(001)R45°$ we made a body cubic tetragonal (bct) Cu structure from Cu^{fcc} rotated by 45° as is shown in Figure 1. Employing the new $a' = b' = 2.560$ Å cell parameters for Cu network, we obtained a $W(001)/Cu^{fcc}(001)R45°$ of size (5.75 Å × 5.75 Å × 6.81N Å) before geometry optimizations.

For each model of the interface $W(001)/Cu^{bcc}(001)$ and $W(001)/Cu^{fcc}(001)R45°$, we determined the energy of the interface (E_{int}) and the work of separation (W_{sep}) using equations (1) and (2) respectively:

$$E_{int} = \frac{E_{W/Cu} - E_{W_{bulk}} - E_{Cu_{bulk}}}{2A}, \quad (1)$$

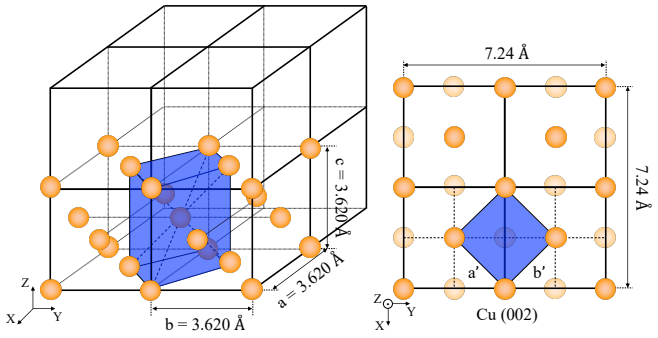

Figure 1: Construction of Cu^{bct} bulk from the Cu^{fcc} structure. The blue volume represents the Cu^{bct} unit cell employed at the $W(001)/Cu^{fcc}(001)R45°$. In the right panel, we show the crystallographic plane (002) where the light orange balls correspond to the position of the Cu atoms in the crystallographic plane (004).

$$W_{\text{sep}} = \frac{E_{\text{W}} + E_{\text{Cu}} - E_{\text{W/Cu}}}{2\text{A}}, \tag{2}$$

In equation (1), $E_{\text{W/Cu}}$ is the energy of the W/Cu working-cell, $E_{\text{W}_{bulk}}$ and $E_{\text{Cu}_{bulk}}$ are the energy of W and Cu bulks, while A is the surface area of the W/Cu interface. In equation (2), E_{W} and E_{Cu} are the energies of the remaining W or Cu bulk once the Cu or W part is removed from the interface. The optimal number of cells in the Z direction $n_z = 2\text{N}$ was chosen such that E_{int} and W_{sep} falls below 1 meV/Å^2 with respect to the larger super-cell $(2 \times 2 \times 14)$ here considered.

3 Results and discussion

3.1 Model of the interface

Full relaxations were conducted for both interface models depending on the number of layers N in the Z direction. In a plane parallel to the interface, it resulted in identical changes of the a and b cell parameters along the X and Y directions. Perpendicular to the interface, geometry relaxations led to an inter-layer distance c that varies along the Z direction. These variations are shown in Figure 2 for various N. In each cell whose number is displayed in the abscissa of Figure 2, the c parameter converges starting from $\text{N} = 3$ resulting in a $(2 \times 2 \times 6)$ interface model. In the end, the most noticeable result is that both $W(001)/Cu^{bcc}(001)$ and $W(001)/Cu^{fcc}(001)R45°$ models converged to the same final minimum energy structure, which geometry and symmetry are analyzed hereafter.

The values of E_{int} and W_{sep} are 0.069 eV/Å^2 (1.11 J/m^2) and 0.266 eV/Å^2 (4.26 J/m^2), respectively, for the largest $(2 \times 2 \times 14)$ interface model here considered. Starting from $\text{N} = 4$, E_{int} and W_{sep} are well converged to 0.068 eV/Å^2 (1.09 J/m^2) and 0.266 eV/Å^2 (4.26 J/m^2), respectively. As a consequence, we selected the number of layers $\text{N} = 4$ consistent with the $(2 \times 2 \times 8)$ interface model that leads to a well-converged working-cell. For this working-cell, a and b parameters converge to 3.162 Å, close to their value in perfect W at 3.187 Å. It means that at the interface, W imposes the geometry of the whole structure in the X and Y planes, leading to an expansion of the Cu network. The reverse was observed in the Z direction: the inter-layer distance of Cu compresses to c = 2.531 Å while W expands to c = 3.210 Å.

Bodlos et al. [18] determined $E_{\text{int}} = 0.71$ J/m^2, but on a different interface orientation W(110)/Cu(111). Liang et al. [13] calculated $W_{\text{sep}} = 4.57$ J/m^2 and $E_{\text{int}} = 0.76$ J/m^2 on the same interface investigated

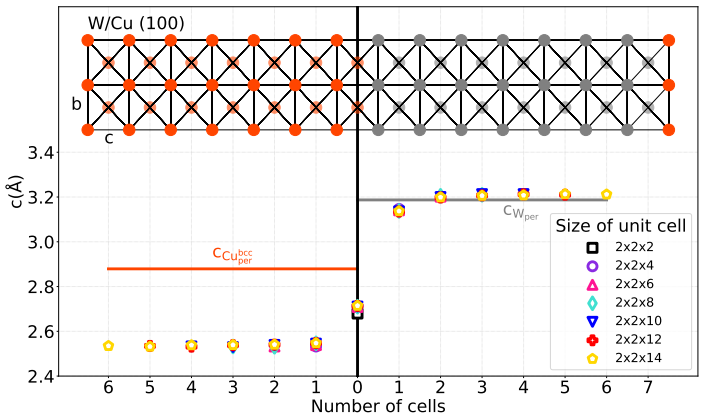

Figure 2: Inter-layer distance c in the Z direction of the W/Cu super-cell. The black line displays the interface. We numbered the layers starting from the interface. Above the graph, we schematically represent the (100) crystallographic plane of the $(2 \times 2 \times 14)$ W/Cu: the orange and gray points are the positions of Cu and W atoms, respectively. The light-orange and light-gray points represent the positions of Cu and W atoms in the (200) plane, respectively. The horizontal orange and gray lines the c parameter of Cu^{bcc} and W^{bcc} respectively: $c_{Cu^{bcc}} = 2.871$ Å and $c_{W^{bcc}} = 3.187$ Å.

here Cu(100)/W(100). These values are close to the ones we calculated: $W_{sep} = 4.26$ J/m^2 and $E_{int} = 1.09$ J/m^2. The difference is probably due to the fact that Liang et al. [13] did not performed any volume relaxation but kept the cell parameter fixed to the one imposed by the tungsten substrate. In addition they used a (1×1) unit-cell in the (X, Y) plane, which does not allow tungsten and copper to reconstruct.

3.2 Reconstructed structure of the interface

We now have defined a well-converged $(2 \times 2 \times 8)$ interface model and focus on its reconstructed structure and geometry. Figure 3a and 3b represent the Cu and W layers at the interface before and after geometry optimization respectively. W is the stiffer material and it keeps the same bcc structure as in the pure metal. However, at the interface, W atoms in the first layer in contact with the Cu network moves a bit (blue arrows in Figure 3b and 3c) from their equilibrium position to adopt a zig-zag structure which does not propagate deeper into the W layers. The displacement of the Cu atoms of the interface is more pronounced, and the distortion propagates into the full Cu structure. Figure 3c displays a larger view of how the atoms are displaced at the interface. It is to be compared with Figure 3d that represents a $Cu^{hcp}(11\bar{2}0)$ structure deposited on top of $W^{bcc}(001)$ surface, with the [1100] direction of Cu^{hcp} collinear to the [110] direction of W^{bcc}. $Cu^{hcp}(11\bar{2}0)$ is a little bit distorted such as to match with the W^{bcc} network. Such a structure was experimentally observed by Wormeester et al. [6] and Bollmann et al. [8] for Cu deposited on top of W(001).

The hcp reconstruction propagates into the full Cu structure from one W/Cu interface to the other one in the $(2 \times 2 \times 8)$ working-cell. In order to check this propagation is not an artifact of having two W/Cu interfaces into the model, we fixed the atoms at the second interface (shown for N = 7 in Figure 2) to their bcc(001) structure, and let the W/Cu interface in the middle of the working-cell (black line in Figure 2) free to move. The hcp reconstruction propagates similarly up to the fixed layer of the frozen W/Cu interface. This indicates the W(001) surface induces a hcp reconstruction into Cu. This minimizes the mismatch between the W and Cu networks and ends-up in a $W^{bcc}(001)/Cu^{hcp}(11\bar{2}0)$ interface.

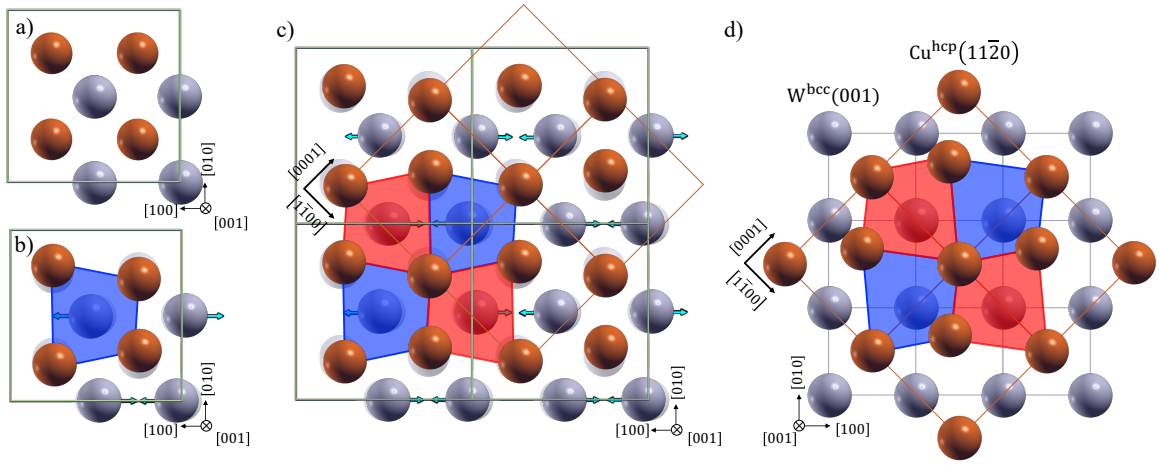

Figure 3: Reconstruction of the Cu network. a) Before geometry relaxation, b) after geometry relaxation, c) same as b) but at a larger scale, and d) the $Cu^{hcp}(11\bar{2}0)$ on W(100) experimentally observed by Wormeester et al. [6] and Bollmann et al. [8]. The blue and red surfaces represent the regions with similar deformations.

3.3 Effect on the charge density

The hcp reconstruction is shown in Figure 4 in the (010) plane: the top part of Figure 4 shows the undistorted structure while the lower part shows the minimum energy $Cu^{hcp}(11\bar{2}0)/W^{bcc}(001)$ interface. The reconstruction clearly induces two different channels along the [001] direction in between the Cu atoms: one channel is narrower while the other one is wider as compared to the undistorted structure. It is expected that these two channels will interact differently with hydrogen isotopes when they will diffuse through the interface.

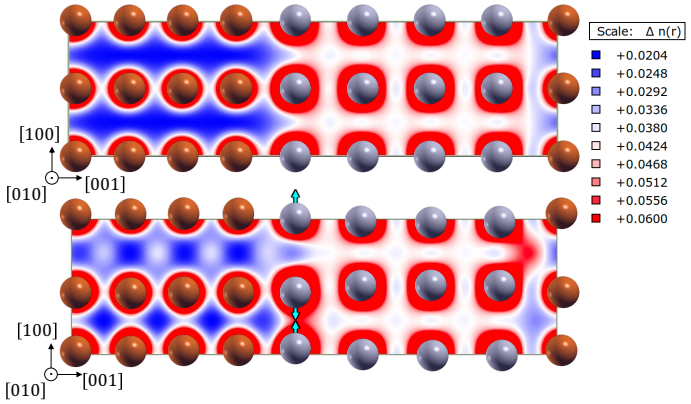

Figure 4: Charge density along the $(2\times2\times8)$ W/Cu working cell. The top and bottom representations correspond to the (010) crystallographic plane before and after relaxation, respectively.

A good indicator of where hydrogen atoms resides in a materials is given by the electronic density. Indeed it already proved to be an efficient tool to predict the location of minimum energy interaction with hydrogen [19–22]. To this end, Figure 4 displayed the electronic density in the (010) plane of the interface model. The regions of low charge density are located in the Cu network at the plane of the interface with a value of 0.0204 a.u. In the W network, the regions of low charge density have a value

of 0.0380 a.u. approximately. The electron density of a homogeneous electron gas that minimizes its interaction with a hydrogen atom is $n_0 = 0.0026$ a.u. ≈ 0.018 eÅ^{-3} [23]. As the electronic densities above mentioned are higher than n_0, it is expected that hydrogen resides in locations of minimum electronic densities. It follows that the solutions energy will be lower (and the solubility of hydrogen higher) in the Cu part rather than in the tungsten part of the interface. The locations of low charge density in the Cu network correspond to octahedral sites, which according to the bibliography is the most stable position for the H atoms in the Cu bulk [24–26]. In the case of the W network, the regions of lowest charge density correspond to tetrahedral sites, which are the positions where the solution energy of H is the lowest in W bulks [14, 27, 28]. Nevertheless, at the plane of the interface, the charge density takes its minimum value, which indicates a possible accumulation of hydrogen there.

4 Conclusions

In this work, an atomic-scale model of the W/Cu interface was built. The size of the working-cell was defined to $(2 \times 2 \times 8)$, which makes converge W_{sep}, E_{int} and the inter-layer distance c. We built two different crystallographic orientations W(001)/Cu$^{\text{bcc}}$(001) and W(001)/Cu$^{\text{fcc}}$(001)R45° that minimizes the mismatch between both Cu and W networks. After geometry relaxation, the Cu networks of both systems reconstruct, leading to the same W$^{\text{bcc}}$(001)/Cu$^{\text{hcp}}$(11$\bar{2}$0) final structure. This reconstruction affect the charge density which led us to conclude that the interface is a possible place of high solubility for HIs.

5 Acknowledgments

This work is supported by Région PACA. It has been carried out within the framework of the EUROfusion Consortium, funded by the European Union via the Euratom Research and Training Programme (Grant Agreement No 101052200 — EUROfusion). Views and opinions expressed are however those of the author(s) only and do not necessarily reflect those of the European Union or the European Commission. Neither the European Union nor the European Commission can be held responsible for them. The authors were granted access to the high-performance computing resources of IDRIS under Allocation No. A0120806612 made by Grand Equipement National de Calcul Intensif and to the Marconi Supercomputer at CINECA Super Computing Application and Innovation Department, Bologna, Italy.

References

[1] D. Perrault. "Safety issues to be taken into account in designing future nuclear fusion facilities". *Fusion Engineering and Des.* 109.111 (2016), pp. 1733–1738. URL: https://doi.org/10.1016/j.fusengdes.2015.10.012.

[2] E. A. Hodille et al. "Estimation of the tritium retention in ITER tungsten divertor target using macroscopic rate equations simulations". *Phys. Scr.* 170 (2017), pp. 14033–14040. DOI: 10.1088/1402-4896/aa8787.

[3] M. Missirlian et al. "The WEST project: current status of the ITER-like tungsten divertor". *Fusion Engineering and Des.* 89.7-8 (2014), pp. 1048–1053.

[4] T. Hirai et al. "Use of tungsten material for the ITER divertor". *Nucl. Mater. and Energy* 9 (2016), pp. 612–622. URL: https://doi.org/10.1016/j.nme.2016.07.003.

[5] E. Bauer et al. "Adsorption and condensation of Cu on W single-crystal surfaces". *J. Appl. Phys.* 45.12 (2003), pp. 5164–5175. URL: https://doi.org/10.1063/1.1663211.

[6] H. Wormeester et al. "Growth of hcp Cu on W (100)". *Surf. Sci.* 377 (1997), pp. 988–991.

[7] B. L. Bramfitt. "The effect of carbide and nitride additions on the heterogeneous nucleation behavior of liquid iron". *Metallurgical Transactions* 1 (1970), pp. 1987–1995. URL: https://doi.org/10.1007/BF02642799.

[8] T. R. J. Bollmann et al. "Growth and decay of hcp-like Cu hut-shaped structures on W(100)". *Phys. Rev. B* 85 (12 Mar. 2012), p. 125417. DOI: 10.1103/PhysRevB.85.125417.

[9] P. Giannozzi et al. "Advanced capabilities for materials modelling with Quantum ESPRESSO". *J.Phys.: Condens. Matter* 29.46 (2017), p. 465901. DOI: 10.1088/1361-648X/aa8f79.

[10] J. P. Perdew, K. Burke, and M. Ernzerhof. "Generalized Gradient Approximation made simple". *Phys. Rev. Lett.* 77.18 (1996), pp. 3865–3868. URL: https://doi.org/10.1103/PhysRevLett.77.3865.

[11] N. Fernandez, Y. Ferro, and D. Kato. "Hydrogen diffusion and vacancies formation in tungsten: density functional theory calculations and statistical models". *Acta Materialia* 94 (2015), pp. 307–318.

[12] H. Wormeester, E. Hüger, and E. Bauer. "hcp and bcc Cu and Pd films". *Phys. Rev. Lett.* 77.8 (1996), p. 1540.

[13] C. P. Liang et al. "Interface structure and work function of W-Cu interfaces". *Appl. Phys. Lett.* 103.21 (2013), p. 211604. URL: https://doi.org/10.1063/1.4833249.

[14] G. C. Ma, J. L. Fan, and H. R. Gong. "Fundamental effects of hydrogen on cohesion properties of Cu/W interfaces". *Solid State Communications* 250 (2017), pp. 79–83. URL: https://doi.org/10.1016/j.ssc.2016.11.018.

[15] Q. Yang et al. "Influence of Cu/W interfacial structure on the resistance against harmful helium atoms: A mechanism analysis". *J. Alloy. and Compd.* 903 (2022), p. 163817. URL: https://doi.org/10.1016/j.jallcom.2022.163817.

[16] Z. A. Piazza et al. "Saturation of tungsten surfaces with hydrogen: A density functional theory study complemented by low energy ion scattering and direct recoil spectroscopy data". *Acta Materialia* 145 (2018), pp. 388–398. URL: https://doi.org/10.1016/j.actamat.2017.12.029.

[17] Z. A. Piazza et al. "Predictive atomistic model for hydrogen adsorption on metal surfaces: Comparison with low-energy ion beam analysis on tungsten". *The Journal of Physical Chemistry C* 125.29 (2021), pp. 16086–16096. URL: https://doi.org/10.1021/acs.jpcc.1c01068.

[18] R. Bodlos et al. "Energies and structures of Cu/Nb and Cu/W interfaces from density functional theory and semi-empirical calculations". *Materialia* 21 (2022), p. 101362.

[19] Y. L. Liu et al. "Vacancy trapping mechanism for hydrogen bubble formation in metal". *Phys. Rev. B* 79.17 (2009), p. 172103.

[20] L. Yang and B. D. Wirth. "Surface stability and H adsorption and diffusion near surfaces of W borides: a first-principles study". *Nuclear Fusion* 63.6 (2023), p. 066002. DOI: 10.1088/1741-4326/acc6de.

[21] L. Yang and B. D. Wirth. "First-principles study of hydrogen behavior near W/WC interfaces". *Journal of Applied Physics* 127.11 (2020), p. 115107. URL: https://doi.org/10.1063/1.5141761.

[22] L. Yang and B. D. Wirth. "First-principles study of hydrogen diffusion and self-clustering below tungsten surfaces". *Journal of Applied Physics* 125.16 (2019), p. 165105. URL: https://doi.org/10.1063/1.5092595.

[23] M. J. Puska, R. M. Nieminen, and M. Manninen. "Atoms embedded in an electron gas: Immersion energies". *Phys. Rev. B* 24.6 (1981), p. 3037. URL: https://doi.org/10.1103/PhysRevB.24.3037.

[24] W. Eichenauer, W. Löser, and H. Witte. "Löslichkeit und Diffusionsgeschwindigkeit von Wasserstoff und Deuterium in Einkristallen aus Nickel und Kupfer". *J. Mater. Res.* 56.5 (1965), pp. 287–293. URL: https://doi.org/10.1515/ijmr-1965-560504.

[25] H. Wenzl. "Properties and applications of metal hydrides in energy conversion systems". *International Met. Rev.* 27.1 (1982), pp. 140–168. URL: https://doi.org/10.1179/imr.1982.27.1.140.

[26] H. B. Zhou, Y. Zhang, and X. Ou. "Dissolution and diffusion behaviors of hydrogen in copper: A first-principles investigation". *Comp. Mater. Sci.* 79 (2013), pp. 923–928. URL: https://doi.org/10.1016/j.commatsci.2013.08.002.

[27] R. Frauenfelder. "Solution and Diffusion of Hydrogen in Tungsten". *J. Vac. Sci. and Technol.* 6.3 (1969), pp. 388–397. URL: https://doi.org/10.1116/1.1492699.

[28] H. B. Zhou et al. "Investigating behaviours of hydrogen in a tungsten grain boundary by first principles: from dissolution and diffusion to a trapping mechanism". *Nucl. Fusion* 50.2 (2010), p. 025016. DOI: 10.1088/0029-5515/50/2/025016.